Exchange-coupling properties of $La_{1-x}Ca_xMnO_3$ ferromagnetic/antiferromagnetic multilayers

N. Moutis
Institute of Materials Science, National Center for Scientific Research "Demokritos," 153 10 Aghia Paraskevi Athens, Greece

C. Christides
Department of Engineering Sciences, School of Engineering, University of Patras, 26 110 Patras, Greece

I. Panagiotopoulos and D. Niarchos
Institute of Materials Science, National Center for Scientific Research "Demokritos," 153 10 Aghia Paraskevi Athens, Greece
(Received 31 March 2001; published 14 August 2001)

Compositionally modulated structures consisting of $La_{1-x}Ca_xMnO_3$ ferromagnetic (FM) layers ($x=0.33$, 0.4, 0.48) and $La_{1-y}Ca_yMnO_3$ antiferromagnetic (AF) layers ($y=0.52$, 0.67, 0.75) were grown on (001)$LaAlO_3$ by pulsed laser deposition. Thermomagnetic and isothermal magnetic, magnetotransport measurements reveal an exchange biasing mechanism below a blocking temperature $T_B \approx 70$ K. Between 5 K and T_B, the observed exponential thermal decay of coercive (H_c) and exchange biasing (H_{EB}) fields follows the drop of magnetization (M_{FC}) in the field-cooling curves. All the experimental results indicate that thermal fluctuations, different from spin-wave demagnetization, give rise to exponential thermal decay of M_{FC} and determine the observed behavior of H_c and H_{EB} at low T. The extrapolated values of H_c and H_{EB} to zero temperature exhibit a quasilinear dependence on the average interfacial concentration $\xi=(x+y)/2$, both decreasing for fixed $y=0.67$ while x increases or both increasing for fixed $x=0.4$ while y increases.

DOI: 10.1103/PhysRevB.64.094429 PACS number(s): 75.70.Cn, 81.15.Fg, 72.15.Gd, 75.30.Gw

I. INTRODUCTION

Exchange bias is associated with the unidirectional anisotropy created at the interface between a ferromagnetic (FM) and an antiferromagnetic (AF) material when they are in intimate contact with each other so as to be exchange coupled. Exchange biasing is manifested[1] as a displacement of the loop of the soft (FM) layer along its field axis and an increase of coercivity or width of its hysteresis loop. This loop shift is important because the exchange coupling can be used to ''pin'' the FM soft layers in the low fields used in spin valves[2] and magnetic random access memories.[3,4] However, despite the technological interest in these structures there is little basic understanding of the phenomenon.[5]

Of special interest is the interface spin structure in the AF layer.[1,6] One characteristic length scale is the size of the magnetic domains in both FM and AF layers of exchange-coupled bilayers.[7,8] Another fundamental parameter is the strength of the exchange coupling at the AF/FM interface J_{eb}. In systems[7] with clearly defined AF/FM interfaces, where the AF spins are fixed and the FM spins across the layer are uniform, the exchange coupling across a FM/AF interface is such that the moments in the AF material lie on an axis that is *orthogonal* to the FM moment at the time of cooling through the Néel temperature T_N. During field cooling (FC) this magnetic moment configuration gives rise to an exchange field (H_{EB}) parallel in the direction of the FM moment (M_s) that establishes[9] a preferred *direction* of magnetization at the interface. If the thickness of the FM layer (t_F) is less than the thickness of a domain wall (δ_{dw}) or an exchange length, then in the strong-AF limit ($K_A t_A \gg J_{eb}$) the response of the FM layer to a field causes an exchange twist of spins in the AF layer near the interface.[7] In this approximation, the H_{EB} can be modeled as[8]

$$H_{EB} = -2\frac{K_A \delta_A}{M_s t_F} \approx -\frac{\sigma_{dw}^A}{2M_s t_F}, \tag{1.1}$$

where $\delta_A = \pi(A_{AF}/K_A)^{1/2}$ is the thickness of a domain wall in the AF layer, K_A is the magnetic anisotropy coefficient, $\sigma_{dw}^A = (A_{AF}K_A)^{1/2}$ is the energy of a domain wall in the AF layer, and A_{AF} is the exchange stiffness constant.

Recently we reported[10,11] the existence of exchange biasing on multilayers with alternating layers of FM $La_{2/3}Ca_{1/3}MnO_3$ and AF $La_{1/3}Ca_{2/3}MnO_3$ compositions. A later study investigated[12] $La_{0.67}Ca_{0.33}MnO_3$(FM)/$La_{0.5}Ca_{0.5}MnO_3$(AF) bilayers with specially designed interfacial structures that affect the exchange coupling. These studies[10–12] reveal that exchange bias appears below a blocking temperature (T_B) which is much less than the magnetic ordering temperatures of the AF (T_N) and the FM (T_c) layers.

The temperature dependence of exchange bias and coercivity at low T can be modeled by considering two possible factors:[13,14] (i) the temperature dependence of K_A, A_{AF}, and σ_{dw}^A and (ii) thermally activated switching of AF grains. The former has been attributed[13–15] to magnetization reduction that is basically controlled by long-wavelength spin waves at low T. The latter causes there to be a blocking temperature T_B that is well below the T_N. Above the T_B the AF order in the grains is not stable[13] and no unidirectional anisotropy (exchange bias) develops. Below the T_B the AF order becomes stable and the unidirectional anisotropy at low T depends[13] on the ratio of the average interfacial coupling energy to the domain wall energy. Also, it was observed[14,15]

that exchange-coupled layers with a $T_B < T_N$ exhibit assymetric hysteresis loops due to irreversible transitions of the AF order in the AF grains.

In this study we measure the temperature dependence of coercivity, exchange biasing field, and magnetoresistance in a series of La-Ca-Mn-O AF/FM multilayers where the interfacial composition is intentionally modified by changing the Ca concentration in the FM and the AF layers. Our intent is, first, to investigate the interplay between the thermomagnetic fluctuations of AF grains and the increasing density of AF interfacial uncompensated spins[14,16] at low temperatures and, second, to isolate the intrinsic physical property that determines the temperature dependence of H_{EB} and H_c below the T_B.

II. EXPERIMENTAL DETAILS

The multilayers were prepared by pulsed-laser deposition (PLD) of bulk stoichiometric targets on (001)$LaAlO_3$ single-crystal substrates. The beam of an LPX105 eximer laser (Lambda Physic), operating with KrF gas ($\lambda = 248$ nm), was focused on a rotating target. During deposition the substrate temperature was stabilized at 700 °C and the oxygen pressure in the chamber was 0.3 Torr, resulting in a deposition rate of 0.03 nm per pulse. Two series of $[La_{1-x}Ca_xMnO_3(\Lambda/2)(FM)/La_{1-y}Ca_yMnO_3(\Lambda/2)(AF)]_{15}$ multilayers were used to investigate the effect of the Mn^{3+}:Mn^{4+} interface ratio $[2-x-y]$:$[x+y]$ in the exchange biasing properties. The bilayer thickness Λ is chosen to be about 8 nm, where the optimum biasing effect was observed.[10] One series is grown with constant $y = 0.67$ while $x = 0.33$, 0.4, 0.48, and the other with constant $x = 0.4$ while $y = 0.52$, 0.67, 0.75. Both series were deposited on a 40-nm-thick AF buffer layer. For brevity, we named the samples by the Ca concentration ratio x/y used.

III. RESULTS

A. X-ray diffraction

X-ray diffraction (XRD) spectra were collected at ambient conditions with a Siemens D500 diffractometer using Cu $K\alpha$ radiation. The existence of the superstructure is confirmed by the presence of low-angle superlattice Bragg-peaks and multiple satellite peaks (Fig. 1) around the (001), (002), and (003) Bragg reflections in XRD spectra. Since for all the examined samples there are no traces of mixed (001) and (110) textures, then cumulative roughness effects can be excluded. The grouping of the satellite peaks observed (Fig. 1) nearby the (00l) Bragg positions of the $LaAlO_3$ substrate indicates that there is a coherent AF/FM superlattice. Also, a multiplet of asymmetric peak intensities appears around the zeroth-order (00l) peaks of the multilayer. Such an asymmetric intensity of the satellite peaks has been reported in multilayers that exhibit chemical and/or strained interfacial profiles along the growth direction.[17] Also, it is worth mentioning that selected area electron diffraction images from cross section transmission electron microscopy[18] reveal epitaxial growth of the compositionally modulated structures.

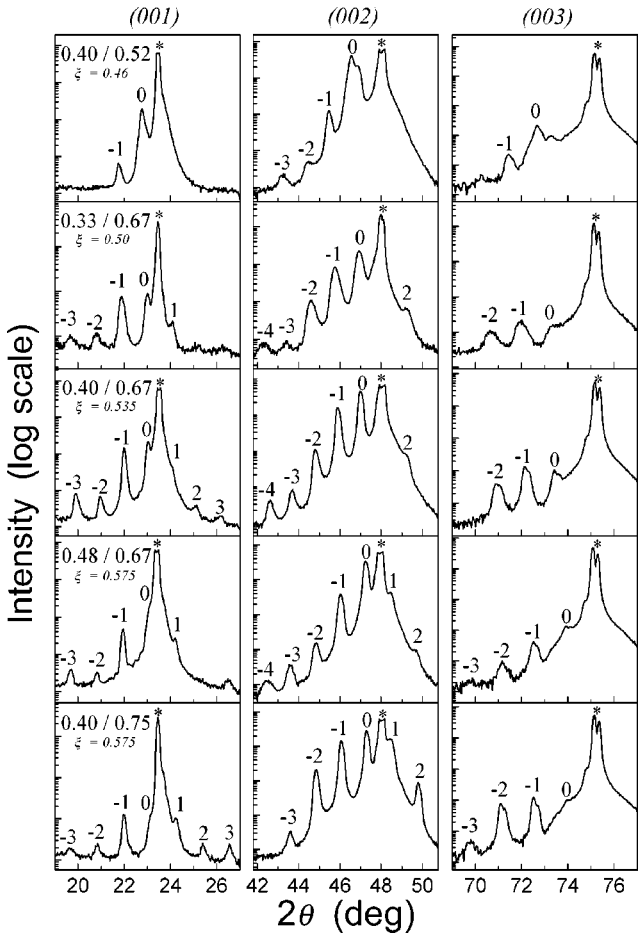

FIG. 1. X-ray diffraction patterns around the (001), (002), and (003) $LaAlO_3$ Bragg peaks (star). The order of the satellite peaks from the AF/FM superstructure is displayed.

B. Magnetic measurements

Magnetic measurements were performed in a Quantum Design MPMSR2 superconducting quantum interference device (SQUID) magnetometer. The coercive and exchange biasing fields were derived from isothermal loops at low temperatures after zero-field cooling (ZFC) from 300 K and FC in 50 kOe. Typical FC and ZFC loops taken at 10 K are shown in Fig. 2. Below 70 K the ZFC loops are symmetric around zero whereas the FC loops are shifted towards negative fields, evidencing an exchange biasing mechanism in all the samples (Table I). The H_{EB} is defined as the loop shift and the H_c as the halfwidth of the loop. Thus, if H_1 and H_2 are the fields for which the descending and ascending parts of a hysteresis loop intercept the abscissa, then $H_{EB} = -(H_1+H_2)/2$ and $H_c = -(H_1-H_2)/2$.

The magnetothermal ZFC and FC curves in Fig. 3 were performed by warming up in 100 Oe after having cooled in zero field and 50 kOe, respectively. The inset of Fig. 3 shows the ZFC curves. In all samples the bifurcation of the FC and the ZFC magnetizations occurs at temperatures T_{bif}, ranging between 155 K and 215 K (Table I), whereas exchange biasing can be detected only below 70 K. Apparently, all the FC curves exhibit a steep decrease of M_{FC} between 5 and 70 K, which defines[10] a blocking or freezing temperature T_B. In

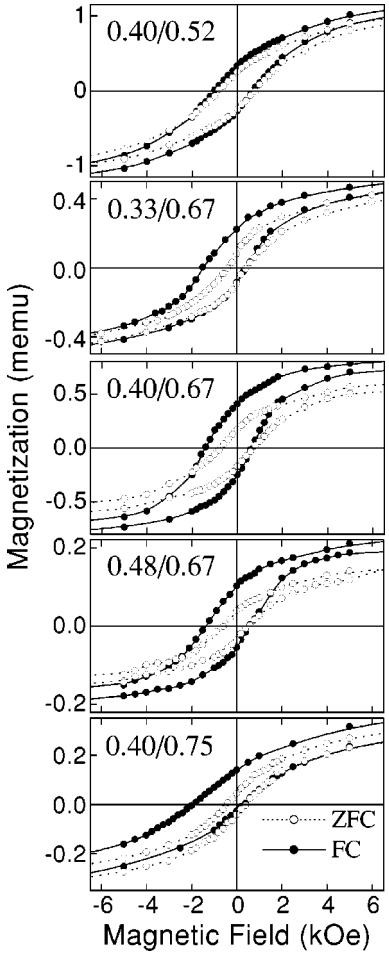

FIG. 2. Magnetic hysteresis loops, measured at 10 K after cooling from 300 K in zero field (open circles) and 50 kOe (solid circles).

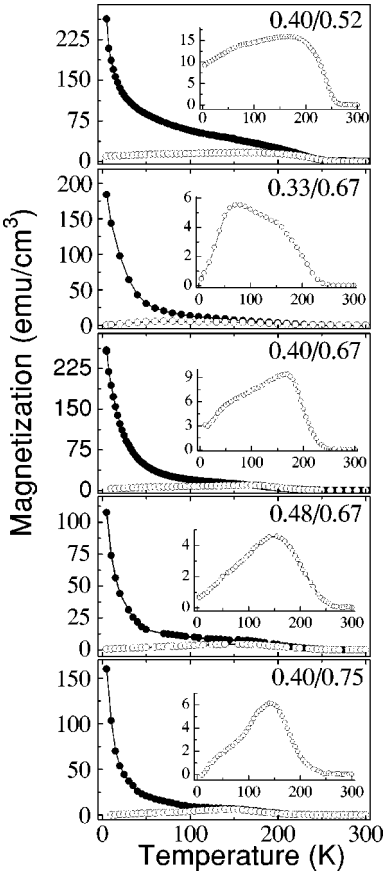

FIG. 3. Magnetothermal measurements, performed by warming up in an applied field of 100 Oe after cooling down from 300 K in zero field (open circles) and 50 kOe (FC, solid circles). For clarity, the insets show the ZFC curves. The magnetization is normalized to the total FM volume of the film used.

particular, the magnitude of the M_{FC} at T_B becomes about 3 times less than the M_{FC} at 5 K whereas the M_{FC} at 5 K is very close to remanent magnetization of the corresponding[19] FM layer. These magnetothermal properties are reminiscent of those observed for an ensemble of fine magnetic grains.[20] Thus, strong thermal fluctuations of magnetic domains are responsible for the observed decrease of magnetic moments in the FM layer. According to the literature[13,8,14] such an effect comes from the coupling of a FM layer, which exhibits uniform magnetization, to a polycrystalline AF layer with small enough AF grains that they do not break up into domains.

Figure 4 shows the variation of H_{EB} and H_c at low temperatures. Both exhibit an exponential rather than a power-law[13,15,14] decrease as a function of temperature. Such an exponential thermal decay of H_c has been observed in some rare-earth pseudobinary compounds[21] and amorphous materials,[22] showing that at low temperatures $H_c(T) = H_c^0 e^{-bT}$ with b a constant and H_c^0 the extrapolation of coercivity at 0 K. Generally, the ground state of the $La_{1-x}Ca_xMnO_3$ system is either FM or AF, depending on Ca doping x, which determines the Mn^{3+}:Mn^{4+} ratio, the phase boundary being at $x \approx 0.5$. In the compositionally modulated multilayers considered here the interfacial Ca concentration x crosses the phase-diagram boundary at $x \approx 0.5$. For $x \approx 0.5$

TABLE I. Typical H_c^{ZFC} values from the ZFC loops at 10 K and H_{EB} and H_c^{FC} values from FC loops with $H_{\mathrm{FC}} = 50$ kOe as a function of $\xi = (x+y)/2$. T_{bif} is the bifurcation temperature from Fig. 2 and T_{C} is the Curie temperature of the film.

x/y	ξ	H_c^{ZFC} (Oe)	H_c^{FC} (Oe)	H_{EB} (Oe)	T_{bif} (K)	T_{C} (K)
0.40/0.52	0.46	790	860	125	215	246
0.33/0.67	0.5	410	960	545	215	215
0.40/0.67	0.535	710	1030	385	185	212
0.48/0.67	0.575	570	955	380	205	224
0.40/0.75	0.575	430	1150	870	155	195

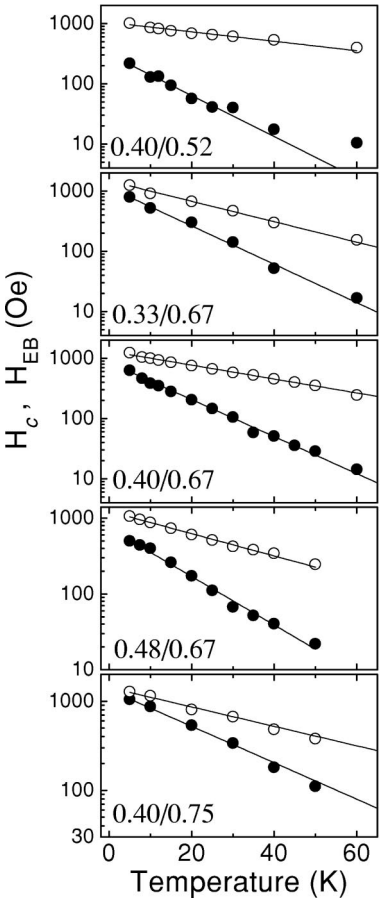

FIG. 4. Temperature dependence of H_{EB} (solid circles) and H_c (open circles) after field cooling in 50 kOe. The solid lines are fits from Eq. (2).

their properties are very sensitive to the application of magnetic fields,[23] affecting both the crystallographic and magnetic phases as a function of temperature. Specifically, the behavior[23] of bulk $La_{1-x}Ca_xMnO_3$, with $x=0.5$ or $x=0.53$, shows that below 200 K a FM and an AF phase coexist microscopically and they transform from one to another as a function of temperature or magnetic field. Furthermore, the AF superexchange (interaction between localized spin moments of Mn^{3+}-Mn^{3+} ions) and the FM double-exchange (transfer of electrons between neighboring Mn^{3+}-Mn^{+4} ions) interactions compete with each other via interface exchange.[24] The existence of frustration due to competing interactions is known to lead to an exponential decay of H_c and H_{EB} as has been observed in amorphous/crystalline $NiFe_2O_4$ ferrite[25] and FM/spin-glass $Ni/Ni_{76}Mn_{24}$ bilayers.[26] Thus, we can fit the observed H_{EB} and H_c (Fig. 4) with

$$H_{EB}(T)=H_{EB}^0\exp(-T/T_1),$$
$$H_c(T)=H_c^0\exp(-T/T_2). \tag{3.1}$$

Figure 5 shows the obtained H_{EB}^0, H_c^0, T_1, and T_2 values against the average (interfacial) Ca nominal composition $\xi=(x+y)/2$. These plots reveal a quasilinear increase (decrease) of H_{EB}^0 and H_c^0 when the Mn^{4+} concentration y increases (is constant) in the AF layers while the Mn^{4+} concentration x is constant (increases) in the FM layers. However, the variation of T_1 and T_2 parameters does not follow a systematic dependence on ξ and their values are less than the observed T_B, where $H_{EB}=0$, in each sample. This result can be associated with a continuous distribution of blocking temperatures due to the statistical distribution of superparamagnetic domains. In support, as-yet unpublished measurements of the so-called[27,28] remanent exchange field in the dc mode provide further experimental evidence for a distribution of T_B's below the bifurcation temperatures in Table I. Since blocking temperature distribution measurements are beyond the scope of this study, they will appear in a forthcoming publication. Accordingly, the same T_B, observed at about 70 K in all the examined samples, indicates that there is a similar distribution of superparamagnetic domains. In NiFe/NiO bilayers[27] such a distribution of local T_B's was related to a variety of exchange paths that is caused by inhomogeneous interfaces due to interfacial disorder and fluctuating atomic arrangement. In our samples, similar interface effects can be related to the induced change of Ca^{2+} concentration from x to y.

To investigate the dependence of H_{EB} and H_c^0 on the H_{FC} a sequence of FC loops has been measured by warming up the sample at 5, 10, 20, 30, 40, 50, 60, and 70 K in six rounds of FC processes. Each sequence uses one of the six $H_{FC}=5$, 10, 20, 30, 40, and 50 kOe. Each loop in a sequence is performed at a maximum field equal to the H_{FC} used. Figure 6(a) shows the temperature dependence of H_1 and H_2 values, where the average film magnetization becomes zero in a FC loop, on each of the H_{FC} used in the 0.40/0.67 sample. Initially, it seems that the dependence of H_{EB} on H_{FC} can be attributed to minor-loop effects. However, in Fig. 6 the H_2 is strongly enhanced below $\sim$70 K by increasing the applied H_{FC} from 5 up to 50 kOe whereas the H_1 is the same, resulting in a constant sum $H_{EB}+H_c^{FC}=H_1$ as a function of H_{FC} at a given temperature. In addition, above 70 K ($\approx T_B$) the H_{EB} approaches zero whereas the H_c^{FC} converges at similar values, indicating that the applied H_{FC} affects in a different way the micromagnetic state only when the exchange biasing is established in the AF/FM interfaces. Thus, we observe that the H_{EB} and the H_c^{FC} values are enhanced at low temperatures. Also, Fig. 6(b) reveals that as the applied H_{FC} decreases there is a lowering of the H_c^{FC} values (inset) and an enhancement of the corresponding H_{EB} values at the same temperature. This shows that the different H_{FC} used in Fig. 6(b) affect the degree of FM alignment in the FM areas below the T_B. Similar results were observed in samples with $\xi\geqslant 0.5$.

C. Magnetotransport properties

Magnetotransport measurements have been carried out with the standard four-point probe method, applying the magnetic field parallel to the current flow direction in the film plane. Figure 7 shows the temperature variation of the normalized resistance, measured in 50 kOe (ρ_H) and in zero applied field (ρ_0). The $\Delta\rho/\rho_H=[\rho_0-\rho_H]/\rho_H$ ratio (solid

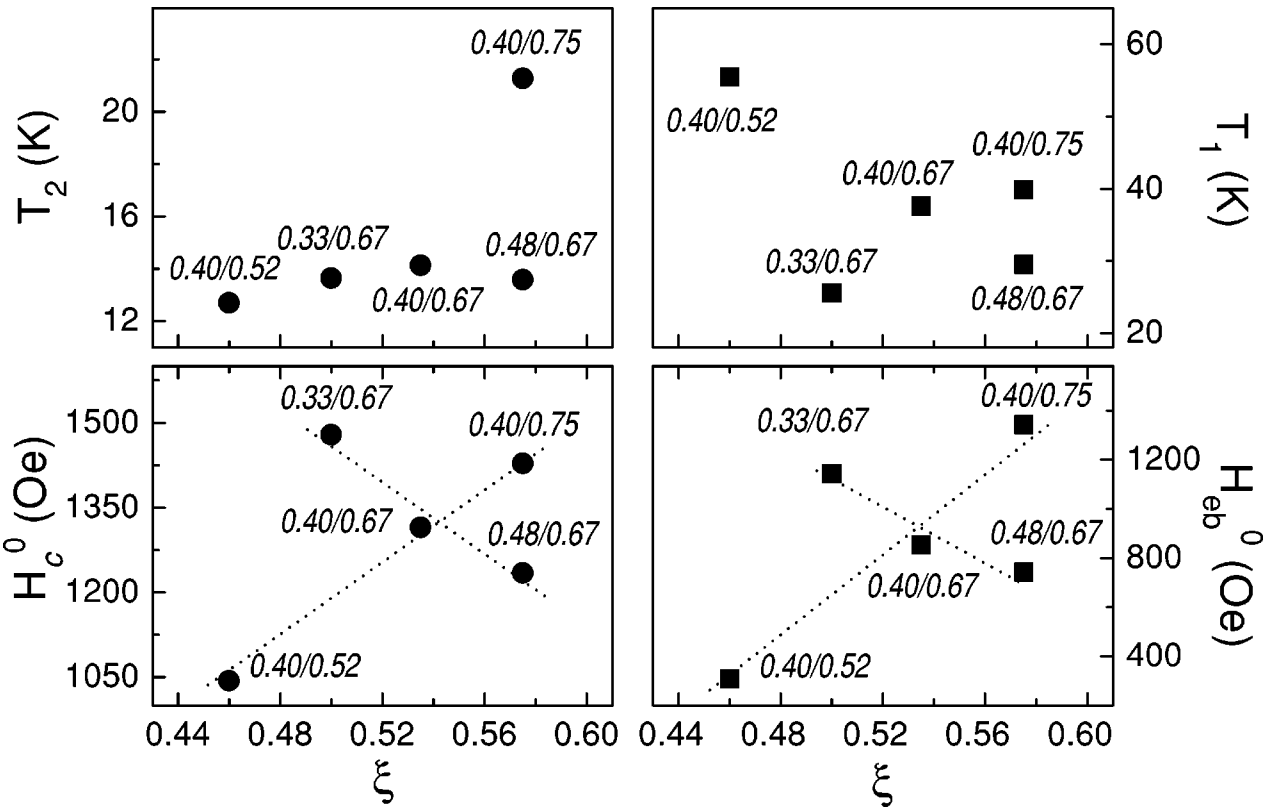

FIG. 5. The obtained values of H_{EB}^0, H_c^0, T_1, and T_2 at $T=0$, after fitting the observed $H_c(T)$ and $H_{EB}(T)$ with Eq. 2, against $\xi=(x+y)/2$. Dotted lines are guides to the eye.

line) gives an estimate of the colossal magnetoresistance (CMR) effect. Apparently, for all samples with $\xi \geq 0.5$, the ZFC resistance decreases steeply by cooling down, spanning several orders of magnitude between 300 and 5 K. Also, the maximum of the resistivity peak occurs below 100 K, where the most drastic change of thermal magnetization appears (Fig. 3), and not around $T_c \approx 250$ K. For the 0.40/0.52 sample ($\xi < 0.5$) the FC-$R(T)$ curve resembles the curves observed in FM (La, Ca)MnO_3 thin films[29] while the normalized ZFC and FC resistances exhibit a difference that is less than an order of magnitude at low T. In contrast, the normalized ZFC and FC resistivities in samples with $\xi \geq 0.5$ exhibit differences that scale between 10 (0.48/0.67) and 10^4(0.40/0.67) times, evidencing a strong AF character at low T. Specifically, the small difference that is observed for the 0.48/0.67 sample indicates that at low T the insulating properties of the coexisting AF phase become dominant as the FM layer stoichiometry approaches the $x=0.5$ region.

In comparison, Fig. 8 shows two indicative cases for the temperature variation of the normalized ZFC resistances, which are obtained from 75-nm-thick films with stoichiometries bounded between the minimum FM ($x=0.33$) and the maximum AF ($x=0.75$) Ca concentrations used. The resistances were normalized at the minimum value in each curve, which is observed at 300 K for $x=0.75$ and at 5 K for $x=0.33$. These two $R(T)$ curves are typical for a single FM layer and a single AF layer with Ca concentrations which are away from the phase separation region with $x=0.5$. It shows qualitatively that the temperature variation of the normalized

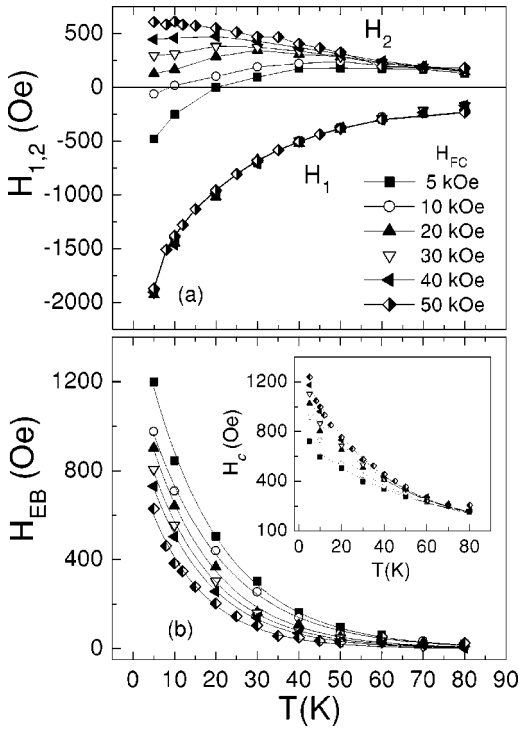

FIG. 6. Sample 0.40/0.67: (a) Temperature dependence of H_1 and H_2 at six different cooling fields. The maximum field in each hysteresis loop is the same as the cooling field used. Lines are guides to the eye. (b) The obtained H_{EB} and H_c (inset) values as a function of temperature for the six different cooling fields. The lines are fits from Eq. (2).

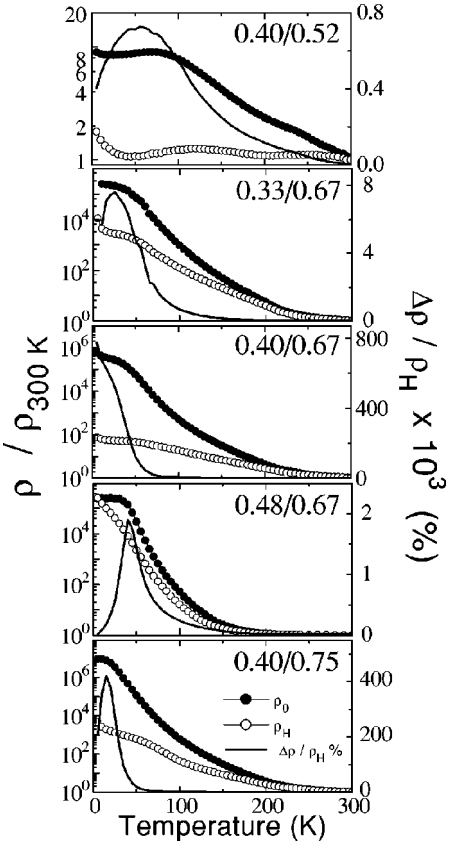

FIG. 7. Resistivity (left axes) normalized to the 300 K value, as a function of temperature, measured in 50 kOe $[R_H(T)]$ and in zero field $[R_0(T)]$. The measurements are taken while heating after cooling in 50 kOe and zero-field cooling, respectively, from 300 K. The obtained values of $\Delta R/R_H$ (solid lines) are shown on the right axes.

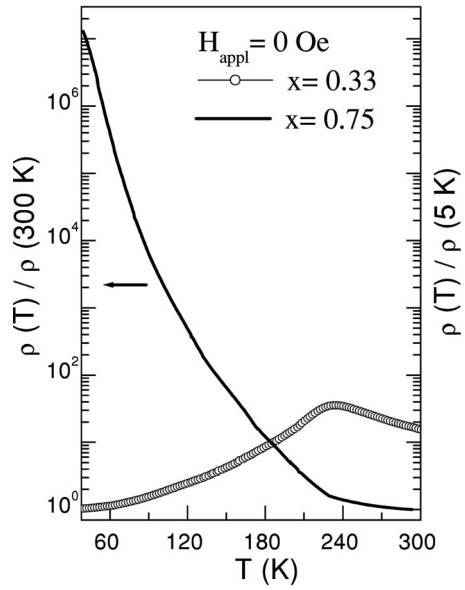

FIG. 8. Semilogarithmic plot of resistivities normalized to their minimum values observed in single AF ($x=0.75$) and FM ($x=0.33$) thin films and measured in zero field as a function of temperature.

resistance of the multilayers (Fig. 7) is governed by the AF layer resistivities at low T. However, quantitatively, the $R(T)$ curves in multilayers are not a simple superposition of the constituent FM and AF layers. The main sources for this change are epitaxial strain[30,31,33] and space charge neutrality at the specific AF/FM interfaces which act as *p-n* junctions between FM layers with hole-type carriers and AF layers with electron-type carriers.[34] Since at low T the FM and the AF phases undergo a phase transformation from pseudocubic high-temperature structures to low-symmetry phases[23,33,35] then below the transition temperature the induced stresses in the multilayer change the balance of charge carriers across the interfaces. Thus, strain-driven effects, which depend strongly on the layer thickness, and the inherent microinhomogeneities[19,23,30–33,36] of manganites, which distinguish them from regular magnetic materials, indicate that the macroscopic properties of single FM or AF thin films cannot be used as a measure of the complex behavior observed in $(La,Ca)MnO_3$ multilayers. In particular, AF-like layers with $x=0.52$ and FM-like layers with $x=0.48$, which are close to the phase boundary with $x=0.5$, exhibit a low-T state which is characterized by the coexistence of FM and AF phases at the microscopic level.[23] Therefore, the low resistivity observed (Fig. 7) between 5 and 300 K in the 0.40/0.52 multilayer and between 150 and 300 K in the 0.48/0.67 multilayer is a consequence of the formation of percolative paths of FM clusters across the film that depend on the average grain sizes in the samples.[36]

To investigate the effect of exchange biasing on the magnetotransport properties we have performed isothermal magnetoresistance (IMR) loops above (at 80 K) and below (at 10 K) T_B. Figures 9, 10, and 11 show FC and ZFC MR loops from the 0.40/0.52, 0.40/0.67, and 0.40/0.75 multilayers, respectively. Plots on the left side show complete ZFC and FC MR loops which are performed between ± 50 kOe. The following are observed.

(1) At 10 K the resistance $R(H)$ is of the order of $10^2\,\Omega$ for the 0.40/0.52 sample, with $\xi<0.5$, exhibiting a small decrease of $R(H)$ in the FC loop relative to the ZFC MR loop. However, for the 0.40/0.67 and 0.40/0.75 multilayers, with $\xi>0.5$, the $R(H)$ is in the range of $10^6\,\Omega$ and the FC loops exhibit a large decrease of $R(H)$ relative to ZFC MR loops.

(2) For low fields at 10 K the ZFC and FC MR loops exhibit an asymmetry between the two branches. Specifically, the ZFC R maximum appears in the negative field range of the descending (from 50 to -50 kOe) field branch whereas in FC loops this R maximum occurs in the positive field range of the ascending (from -50 to 50 kOe) field branch. This asymmetry is more pronounced for the 0.40/0.67 and 0.40/0.75 multilayers. Comparatively, in $La_{0.67}Ca_{0.33}MnO_3$(FM)/$La_{0.5}Ca_{0.5}MnO_3$(AF) bilayers the low-field MR has been attributed[12] to tunneling through the grain boundary region that exhibits an insulating, spin-glass-like magnetic state.

(3) At 80 K the ZFC and FC MR loops become almost identical, exhibiting symmetric branches and much lower hysteresis than at 10 K. However, for the 0.40/0.52 sample

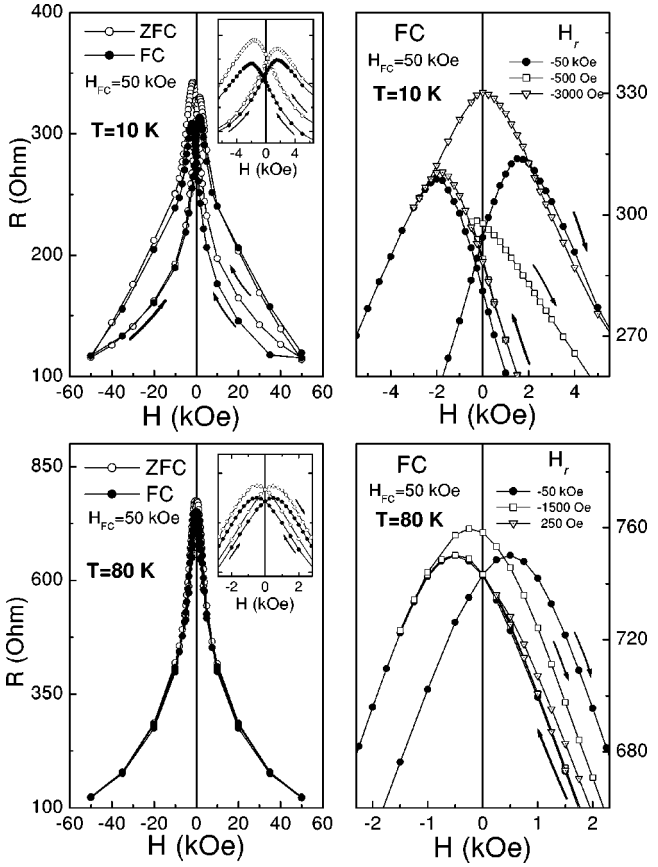

FIG. 9. Sample 0.40/0.52. Left side: *R-H* loops measured at 10 K (above) and 80 K (below) after FC in 50 kOe (solid circles) and ZFC (open circles) from 300 K. The inset shows in detail the observed peaks. Arrows indicate the direction of field change. Right side: *R-H* loops measured at 10 K (above) and 80 K (below) after FC in 50 kOe from 300 K. Incomplete loops (open symbols) measured by varying the field from 50 kOe to H_r and reversing to 50 kOe.

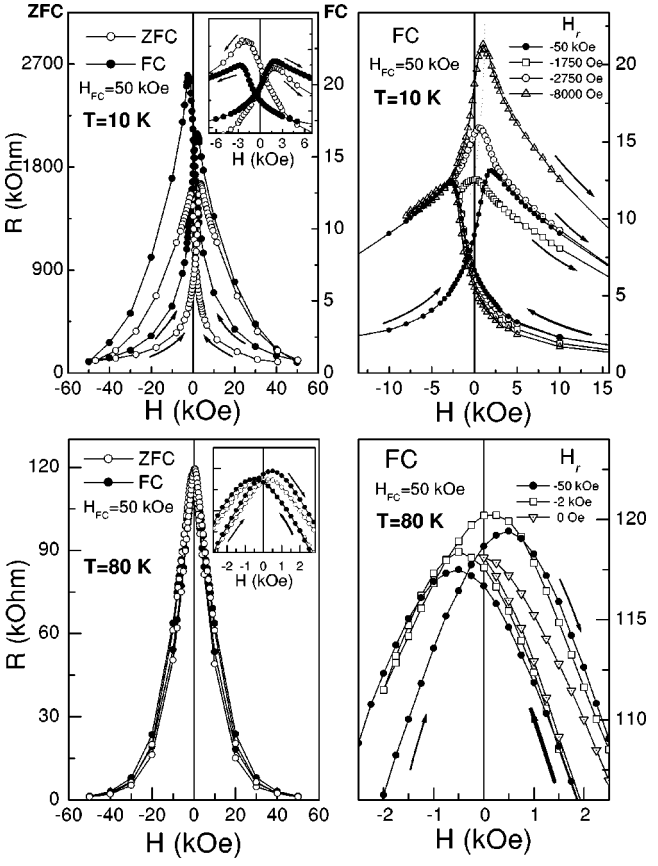

FIG. 10. Sample 0.40/0.67. Left side: *R-H* loops measured at 10 K (above) and 80 K (below) after FC in 50 kOe (solid circles) and ZFC (open circles) from 300 K. The inset shows in detail the observed peaks. Arrows indicate the direction of field change. Right side: *R-H* loops measured at 10 K (above) and 80 K (below) after FC in 50 kOe from 300 K. Incomplete loops (open symbols) measured by varying the field from 50 kOe to H_r and reversing to 50 kOe.

the magnitude of $R(H)$ is enhanced relative to the MR loop at 10 K whereas the 0.40/0.67 and 0.40/0.75 multilayers exhibit a lowering of the $R(H)$ magnitude relative to 10 K.

In Figs. 9, 10, and 11 the plots on the right side show incomplete FC (IMR) loops at 10 and 80 K, where the reversal field (H_r) is much lower than -50 kOe. The main features are the following.

(4) At 10 K the IMR loops exhibit an *R* maximum in the positive field range of the ascending field (from H_r to 50 kOe) branch, alike the complete FC loops. This *R* maximum varies with the H_r value, depending on whether H_r is chosen to be before (H_r^b) or after (H_r^a) the $R(H)$ peak in the descending field (from 50 kOe to H_r) branch. The irreversible IMR branch exhibits an enhancement of $R(H)$, which becomes twice the value of the complete MR loop for the 0.40/0.67 sample (Fig. 10) when the $H_r^a = -8.0$ kOe, evidencing a biasing of the MR loops. It is worth noting that the 0.40/0.67 sample exhibits the maximum (Fig. 2) H_{EB} and H_c^{FC} as well. IMR effects have been reported[12] in exchange-coupled 0.33/0.5 bilayers with large interface roughness, which is induced by the strongly ordered surface structure of the bottom AF layer. Thus, it can be argued that the 40-nm-thick AF-buffer layer, used in our samples, may create such roughness in the multilayer structure at the top.

(5) At 80 K the magnetic irreversibilities are significantly suppressed in the IMR loops. Remarkably, the IMR curves become reversible for H_r^b values.

Since the exchange coupling is an interface effect, the IMR loops indicate that the interfacial resistance becomes dominant at low *T* and the influence of exchange biasing can be clearly observed.[12] Thus, the IMR loops show the pinning effect of the exchange anisotropy on the resistance behavior. These magnetic-history-dependent effects exhibit stronger irreversibilities of IMR than in giant-MR (GMR) loops of Co/Cu/Co structures[37] with strong-AF exchange coupling. The large magnetic irreversibilities, observed in Figs. 9, 10, and 11, show that the origin of exchange coupling below 80 K is interfacial magnetic disorder (like partial domain walls).

IV. DISCUSSION

Today, two of the unsolved issues[1,7,8,13] that are associated with the exchange biasing effect concern the shape and the

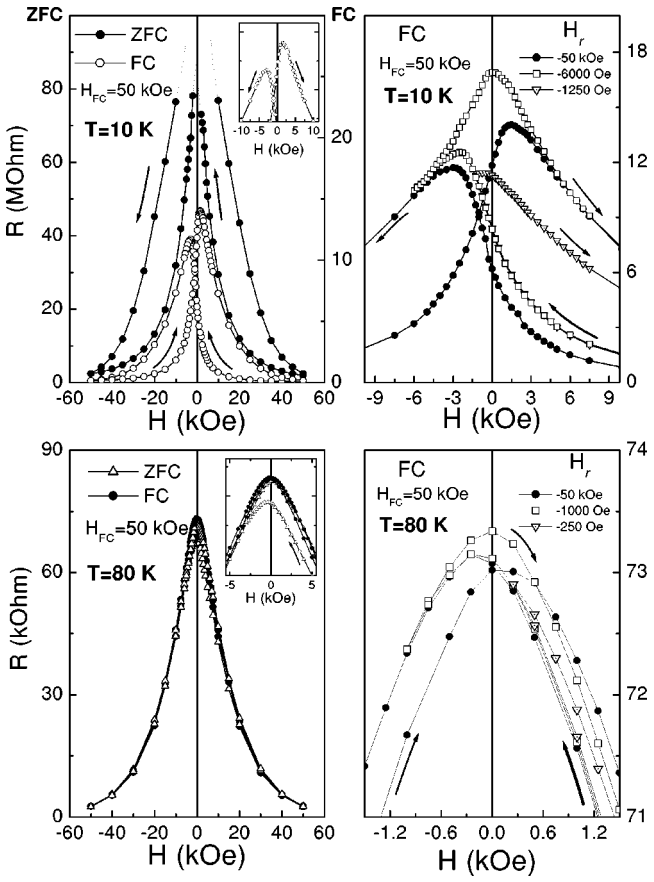

FIG. 11. Sample 0.40/0.75. Left side: *R-H* loops measured at 10 K (above) and 80 K (below) after FC in 50 kOe (solid circles) and ZFC (open circles) from 300 K. The inset shows in detail the observed peaks. Arrows indicate the direction of field change. Right side: *R-H* loops measured at 10 K (above) and 80 K (below) after FC in 50 kOe from 300 K. Incomplete loops (open symbols) measured by varying the field from 50 kOe to H_r and reversing to 50 kOe.

location of the domain wall in the FM or the AF layer. The present study shows that the exchange-coupling properties of $La_{1-x}Ca_xMnO_3$ FM/AF compositionally modulated structures are related (as expected) to these two issues but exhibit an (unexpected) exponential thermal decay. The observed exponential thermal decay cannot be reconciled with a model that is usually applied[8,13,15] for the temperature dependence of exchange-coupling and domain-wall $\sigma^A_{\rm dw}$ energies in the AF layer. This model assumes that the properties of the FM layer and the exchange coupling at the AF/FM interface are temperature independent whereas the $A_{\rm AF}$, $\sigma^A_{\rm dw}$, and K_A parameters in Eq. (1) exhibit thermal demagnetization by long-wavelength spin waves.[13,15]

The major result of this study concerns the thermal variation of $H_{\rm EB}$ and $H_c^{\rm FC}$, which cannot be reconciled with models that use[13,15] spin waves as collective modes of spatially correlated thermal fluctuations in the AF layer. Thus, the exponential thermal decay indicates that the observed magnetic-history-dependent (ZFC, FC) effects and the associated exchange biasing properties can be described by a thermal fluctuation model where short-range ordering or a spin-glass-like[1,25] magnetic disorder is established in AF/FM interfaces. In this section we discuss two alternative ways, one macroscopic and one microscopic, which may account for the unusual exponential thermal decay of $H_{\rm EB}$ and $H_c^{\rm FC}$.

Macroscopically, interfacial magnetic disorder can be introduced by a grain size distribution where both fluctuating and stable AF grains contribute[8,13,14] to coercivity via thermal fluctuations of magnetization. The IMR loops in Figs. 9–11 may imply that the underlying surface roughness[12] of the AF buffer layer creates competing magnetic interactions at the interfaces. In this case, the AF-rich areas in the multilayered structure not only couple with FM-rich areas in the disordered interface but also to the FM adjacent layers, resulting in the observed[1,25] loop shift after field cooling below T_B. However, the systematic dependence of $H^0_{\rm EB}$ and H^0_c (Fig. 5) on ξ indicates that the magnetic disorder in AF/FM interfaces could be of intrinsic nature as well, in addition to an extrinsic part induced by the statistical distribution of superparamagnetic domains. In general, measurements of $M(T)$ can provide useful information about spin-wave excitations in low-dimensional magnetic structures, leading to a microscopic description. A spin-wave theory of exchange-induced anisotropy has interpreted[38] the exchange biasing effect as a self-energy shift of each ferromagnetic spin due to emission and reabsorption of virtual AF spin waves.

Microscopically, the exponential thermal decay of $M_{\rm FC}$ (Fig. 3) can be attributed[39] to critical decay of spin waves into electron-hole pairs due to the tunneling of holes from the FM (hole-type carriers) layers[34] to AF (electron-type carriers) layers in AF/FM interfaces at low *T*. The main reason for the spin-wave damping in these systems is the alteration of exchange coupling that may change the spin-wave energies when the hopping between the FM and AF layer is varied.[39] The theory shows[39] that in ultrathin FM overlayers the spin-wave lifetimes increase substantially as the hopping between the substrate and the overlayer decreases. Thus it can be argued that in $(La,Ca)MnO_3$ multilayers the increase of temperature increases the hopping between the FM and AF layer at the interfaces, causing a rapid decay of spin waves between 5 K and T_B. This scenario is based on the fundamental properties of FM and AF $(La,Ca)MnO_3$ materials. The magnetothermal behavior of $La_{1-x}Ca_xMnO_3$ multilayers originates from the two types[40] of electronic ordering: (i) Jahn-Teller ordering and (ii) charge ordering (CO) of Mn^{3+} and Mn^{4+} ions. Physical reasoning leads us to conclude that layers with more than 50% Mn^{4+} concentration exhibit a transformation to a CO-AF phase below the observed T_B as we cool them down at zero field. Specifically, the ZFC *M* versus *T* (Fig. 3) and *R* versus *T* (Fig. 7) curves provide indirect evidence that a CO-AF, insulating phase stabilizes at low *T*. Also, the results in Fig. 6 show that the percentage of coexisting FM and CO-AF phases depends on the $H_{\rm FC}$ used. Thus, when the CO-AF-insulating phase sets in below 70 K the hopping between AF and FM layers decreases and the spin-wave lifetimes[39] increase substantially as the temperature decreases. This gives a qualitative explanation why the observed (Fig. 3 and 4) thermal decay is faster than the spin-wave demagnetization at low *T*.

Thus far the experiment shows[14,16] that the prerequisite

for the establishment of an exchange biasing mechanism at low T is the observed (Fig. 3) increase of M_{FC}, which always occurs together with the appearance of H_{EB} and the enhancement of H_c below T_B. In our case the observed M_{FC} in Fig. 3 corresponds to the so-called[22] saturation remanence magnetization M_{rs} because it appears after cooling through the T_B in a high field $H_{\mathrm{FC}}=50$ kOe that is subsequently suppressed to 100 Oe at 5 K. Thus, during the warming up process at 100 Oe, the measured M_{FC} is close to the remanent magnetization.

Neel observed[20] an exponential dependence of the M_{rs} on temperature for an ensemble of fine magnetic grains. To explain this, he assumed that the system consists of an ensemble of single-domain grains and for each grain a potential barrier is determined by the anisotropy energy E_a which separates the two easy directions of magnetization. Thermal fluctuations help the magnetization to overcome this barrier within an average time $\tau=\tau_0 \exp(E_a/k_BT)$. A distribution of E_a prevails so that the uncompensated moment M_u of each grain, below its $T_B=E_a/k_B(\ln \tau_m-\ln \tau_0)$, appears frozen in the direction of anisotropy. For $T>T_B$ the domains are superparamagnetic. Assuming that E_a is proportional to the number of moments, N_m, in a domain and that below T_B a domain contributes a moment $M_u=\mu(N_m)^{1/2}$ to M_{rs}, it was shown[41] that the observed exponential dependence of M_{rs} on temperature occurs when the M_u's obey a Gaussian distribution. A distribution of M_u's corresponds to a distribution of grain sizes that creates a distribution of T_B's in superparamagnetic domains. This distribution of T_B's explains why the obtained T_1, T_2 values from Eq. (2) (Fig. 5) cannot be related to the observed blocking temperatures at about 70 K. In parallel, it was found that in NiFe/NiO bilayers[27] the measurable exchange coupling could be described as consisting of the sum of different exchange paths, each with its own local T_B.

Consequently, the only way to realize such a Gaussian distribution of M_u's in our $(\mathrm{La,Ca})\mathrm{MnO_3}$ multilayers is to consider a variety of exchange paths across the AF/FM interfaces,[27] caused by interfacial disorder and fluctuating atomic arrangements of the constituents. In this way, there will be an overall Gaussian distribution of individual probabilities $P(T_{B_i})$, from each exchange path with a local T_{B_i}, which convolutes with a statistical distribution of local unidirectional anisotropies $K_{eb}(T_{B_i})$ to reproduce the observed H_{EB} at every temperature.[27] Thus, the exponential thermal decay (Fig. 4) of H_{EB} and the associated large drop (Fig. 3) of M_{FC} can be attributed to the thermal instability of different exchange paths that behave as superparamagnetic domains above the local T_{B_i}'s. As a result, the ZFC magnetization (Fig. 3, inset) cannot accomplish a preferred direction of magnetic moments at the AF/FM interfaces and the ZFC curves exhibit an almost zero magnetization at 5 K. Thus, after ZFC large fields must be applied subsequently to create a *spin-flop* transition[5] in AF grains which will allow the magnetic moments of FM layers to pass from an almost-zero-magnetization configuration (Fig. 3 inset) at low T to a configuration with a large spontaneous moment in the direction of the field. We have observed that external fields up to 50 kOe were unable to recover the thermoremanent state in the ascending part of the ZFC curves at low T. Our ZFC measurements reveal that thermal activation enables a progressive orientation of film magnetization along the field direction as we approach the T_B from 5 K.

Another distinct feature of the examined multilayers is the observed [Fig. 6(a)] asymmetry of H_1 and H_2 and the associated irreversibilities of IMR loops in Figs. 9–11. Direct experimental observations[8] of the magnetization reversal in exchange-coupled NiO/NiFe bilayers has shown that the thin film remagnetization proceeds by domain-wall nucleation and motion. In this system, the observed[8] asymmetry in the activity of domain nucleation centers of NiO/NiFe bilayers has been attributed either to local variations of AF anisotropy or crystal lattice defects. In parallel, we may assume that this kind of defect[42] can be associated with the asymmetry of H_1 and H_2 observed in our multilayers on application [Fig. 6(a)] of different H_{FC}.

V. CONCLUSIONS

In summary, the observed variation of M_{FC} in Fig. 3 and the results in Figs. 4 and 6(b) indicate that (i) the thermal decay of H_{EB} and H_c^{FC} results from the decay of M_{FC} at low T and (ii) the large drop of M_{FC} in Fig. 3 is due to thermal instability of a statistical distribution of superparamagnetic domains. The dependence of H_{EB}^0 and H_c^0 on ξ (Fig. 5) shows that short-range magnetic ordering dominates at the AF/FM interfaces at low T. The large increase of the low T resistivity, which saturates (Fig. 7) in the temperature range where an increase of M_{FC}, H_{EB}, and H_c^{FC} is observed, indicates a strong localization of charge carriers at low T. The MR and the FC-IMR loops (Figs. 9–11) exhibit loop asymmetries and very large irreversibilities at 10 K which disappear at 80 K, providing clear experimental evidence for the formation of extra domain walls below 80 K due to exchange coupling at the AF/FM interfaces.

[1] J. Nogues and I. K. Schuller, J. Magn. Magn. Mater. **192**, 203 (1999).

[2] B. Dieny, J. Magn. Magn. Mater. **136**, 335 (1994); C. H. Tsang, R. E. Fontana, Jr., T. Lin, D. E. Heim, B. A. Gurney, and M. L. Williams, IBM J. Res. Dev. **42**, 103 (1998).

[3] S. Tehrani, E. Chen, M. Durlam, M. DeHerrera, J. M. Slaughter, J. Shi, and G. Kerszykowski, J. Appl. Phys. **85**, 5822 (1999).

[4] S. S. P. Parkin *et al.*, J. Appl. Phys. **85**, 5828 (1999).

[5] J. Nogues, L. Morellon, C. Leighton, M. R. Ibarra, and I. K. Schuller, Phys. Rev. B **61**, R6455 (2000) and references therein.

[6] H. Ohldag, A. Scholl, F. Nolting, S. Anders, F. U. Hillebrecht, and J. Stohr, Phys. Rev. Lett. **86**, 2878 (2001).

[7] R. C. O'Handley, in *Modern Magnetic Materials* (Wiley, New York, 2000), Chap. 12.2.

[8] V. I. Nikitenko, V. S. Gornakov, L. M. Dedukh, Yu. P. Kabanov, A. F. Khapikov, A. J. Shapiro, R. D. Shull, A. Chaiken, and R. P. Michel, Phys. Rev. B **57**, R8111 (1998).
[9] R. Jungblut, R. Coehoorn, M. T. Johnson, J. aan de Stegge, and A. Reinders, J. Appl. Phys. **75**, 6659 (1994).
[10] I. Panagiotopoulos, C. Christides, M. Pissas, and D. Niarchos, Phys. Rev. B **60**, 485 (1999).
[11] I. Panagiotopoulos, C. Christides, D. Niarchos, and M. Pissas, J. Appl. Phys. **87**, 3926 (2000).
[12] H. B. Peng, X. X. Zhang, Z. Xie, H. J. Tao, B. Xu, H. Liu, and B. R. Zhao, Phys. Rev. B **61**, 8955 (2000).
[13] M. D. Stiles and R. D. McMichael, Phys. Rev. B **60**, 12 950 (1999); **59**, 3722 (1999).
[14] A. F. Khapikov, J. W. Harrel, H. Fujiwara, and C. Hou, J. Appl. Phys. **87**, 4954 (2000).
[15] J. Wang, W. N. Wang, X. Chen, H. W. Zhao, J. G. Zhao, and W. Sh. Zhan, Appl. Phys. Lett. **77**, 2731 (2000).
[16] K. Takano, R. H. Kodama, A. E. Berkowitz, W. Cao, and G. Thomas, Phys. Rev. Lett. **79**, 1130 (1997).
[17] J. Mattson, R. Bhadra, J. B̂. Ketterson, M. Brodsky, and M. Grimsditch, J. Appl. Phys. **67**, 2873 (1990).
[18] C. Christides, N. Moutis, Th. Kehagias, Ph. Komninou, and Th. Karakostas (unpublished).
[19] D. Cao, F. Bridges, D. C. Worledge, C. H. Booth, and T. Gebale, Phys. Rev. B **61**, 11 373 (2000).
[20] L. Neel, Ann. Geophys. (C.N.R.S.) **5**, 99 (1949).
[21] F. T. Parker and H. Oesterreicher, Phys. Status Solidi A **75**, 273 (1983).
[22] K. Moorjani and J. M. D. Coey, *Magnetic Glasses* (Elsevier, Amsterdam, 1984), Chap. VI.
[23] Q. Huang, J. W. Lynn, R. W. Erwin, A. Santoro, D. C. Dender, V. N. Smolyaninova, K. Ghosh, and R. L. Greene, Phys. Rev. B **61**, 8895 (2000).
[24] H. Tanaka and T. Kawai, J. Appl. Phys. **88**, 1559 (2000).
[25] V. Korenivski, R. B. van Dover, Y. Suzuki, E. M. Gyorgy, J. M. Phillips, and R. J. Felder, J. Appl. Phys. **79**, 5926 (1996).
[26] B. Aktas, Y. Oner, and H. Z. Durusoy, J. Magn. Magn. Mater. **119**, 339 (1993).
[27] S. Soeya, T. Imagawa, K. Mitsuoka, and S. Narishige, J. Appl. Phys. **76**, 5356 (1994).
[28] J. P. Nozieres, S. Jaren, Y. B. Zhang, A. Zeltser, K. Pentek, and V. S. Speriosu, J. Appl. Phys. **87**, 3920 (2000).
[29] N.-C. Yeh, R. P. Vasquez, D. A. Beam, C.-C. Fu, J. Huynh, and G. Beach, J. Phys.: Condens. Matter **9**, 3713 (1997).
[30] T. K. Nath, R. A. Rao, D. Lavric, C. B. Eom, L. Wu, and F. Tsui, Appl. Phys. Lett. **74**, 1615 (1999).
[31] T. O'Donnell, M. S. Rzchowski, J. N. Eckstein, and I. Bozovic, Appl. Phys. Lett. **72**, 1775 (1998).
[32] W. Prellier, M. Rajeswari, T. Venkatesan, and R. L. Greene, Appl. Phys. Lett. **75**, 1446 (1999).
[33] V. K. Vlasko-Vlasov, Y. K. Lin, D. J. Miller, U. Welp, G. W. Grabtree, and V. I. Nikitenko, Phys. Rev. Lett. **84**, 2239 (2000).
[34] I. Gordon, P. Wagner, A. Das, J. Vanacken, V. V. Moshchalkov, Y. Bruynseraede, W. Schuddinck, G. Van Tandeloo, M. Ziese, and G. Borghs, Phys. Rev. B **62**, 11 633 (2000).
[35] P. G. Radaelli, D. E. Cox, L. Capogna, S.-W. Cheong, and M. Marezio, Phys. Rev. B **59**, 14 440 (1999).
[36] P. Levy, F. Parisi, G. Polla, D. Vega, G. Leyva, H. Lanza, R. S. Freitas, and L. Ghivelder, Phys. Rev. B **62**, 6437 (2000).
[37] N. Persat, H. A. M. van de Berg, and A. Dinia, Phys. Rev. B **62**, 3917 (2000).
[38] H. Suhl and I. K. Schuller, Phys. Rev. B **58**, 258 (1998).
[39] L. H. M. Barbosa, R. B. Muniz, A. T. Costa, Jr., and J. Mathon, Phys. Rev. B **63**, 174401 (2001).
[40] Y. Tokura and N. Nagaosa, Science **288**, 462 (2000).
[41] J. L. Tholence and R. Tournier, J. Phys. (Paris), Colloq. **35**, C4-229 (1974).
[42] G. H. Yu, C. L. Chai, F. W. Zhu, J. M. Xiao, and W. Y. Lai, Appl. Phys. Lett. **78**, 1706 (2001).